Supplementary Material for

Enhanced wide-angle third-harmonic generation in flat-band engineered quasi-BIC metagratings

Yijia Zang[1], Ruoheng Chai[1], Wenwei Liu[1*], Zhancheng Li[1], Hua Cheng[1*], Jianguo Tian[1], and Shuqi Chen[1,2,3*]

[1] The Key Laboratory of Weak Light Nonlinear Photonics, Ministry of Education, School of Physics and TEDA Institute of Applied Physics, Nankai University, Tianjin 300071, China

[2] School of Materials Science and Engineering, Smart Sensing Interdisciplinary Science Center, Nankai University, Tianjin 300350, China

[3] The Collaborative Innovation Center of Extreme Optics, Shanxi University, Taiyuan 030006, China

*Corresponding author. Email: wliu@nankai.edu.cn; Hua Cheng: hcheng@nankai.edu.cn; Shuqi Chen: schen@nankai.edu.cn

S-I. Analytical derivation of the flat band based on coupled mode theory formalism

The 4×4 Hermitian Hamiltonian H of the metagratings in the main text is given by:

$$H=\begin{pmatrix} \omega_1+v_1k_x & U_1+\kappa_1U_2e^{i\varphi} & V & 0 \\ U_1+\kappa_1U_2e^{-i\varphi} & \omega_1-v_1k_x & 0 & V \\ V & 0 & \omega_2+v_2k_x & U_2e^{i\varphi}+\kappa_2U_1 \\ 0 & V & U_2e^{-i\varphi}+\kappa_2U_1 & \omega_2-v_2k_x \end{pmatrix}. \tag{S1}$$

We define:

$$\begin{cases} C_1=U_1+\kappa_1U_2e^{i\varphi} \\ C_2=U_2e^{i\varphi}+\kappa_2U_1 \end{cases}. \tag{S2}$$

Here, we focus on the dispersion region in the vicinity of the second-order Γ point, where the first-order diffractive coupling process is dominant between the forward and backwards waveguide modes. The eigenvalue $\omega(k_x)$ can be calculated by solving $\det(H-I.\omega)=0$:

$$\begin{aligned}&\mathrm{K}_1^+\mathrm{K}_1^-\mathrm{K}_2^+\mathrm{K}_2^- - \mathrm{K}_1^+\mathrm{K}_1^-\left|C_2\right|^2 - \mathrm{K}_2^+\mathrm{K}_2^-\left|C_1\right|^2 - V^2\left(\mathrm{K}_1^+\mathrm{K}_2^+ + \mathrm{K}_1^-\mathrm{K}_2^-\right) + V^4 - \\ &V^2\left(C_1C_2^* + C_1^*C_2\right) + \left|C_1\right|^2\left|C_2\right|^2 = 0\end{aligned}, \quad \text{(S3)}$$

where $\mathrm{K}_{1,2}^{\pm} = \omega_{1,2} - \omega \pm v_{1,2}k_x$. Equation (S2) is rewritten in the form $\begin{cases} C_1 = A_1 e^{i\Psi_1} \\ C_2 = A_2 e^{i\Psi_2} \end{cases}$ to solve the eigenvalues. We obtain:

$$\begin{cases} A_1 = \sqrt{\kappa_1^2 U_2^2 + U_1^2 + 2\kappa_1 U_1 U_2 \cos\varphi} \\ A_2 = \sqrt{\kappa_2^2 U_1^2 + U_2^2 + 2\kappa_2 U_1 U_2 \cos\varphi} \end{cases}, \quad \text{(S4)}$$

$$\begin{cases} \sin\Psi_1 = \dfrac{\kappa_1 U_2 \sin\varphi}{\sqrt{\kappa_1^2 U_2^2 + U_1^2 + 2\kappa_1 U_1 U_2 \cos\varphi}} \\ \cos\Psi_1 = \dfrac{U_1 + \kappa_1 U_2 \cos\varphi}{\sqrt{\kappa_1^2 U_2^2 + U_1^2 + 2\kappa_1 U_1 U_2 \cos\varphi}} \end{cases}; \begin{cases} \sin\Psi_2 = \dfrac{U_2 \sin\varphi}{\sqrt{\kappa_2^2 U_1^2 + U_2^2 + 2\kappa_2 U_1 U_2 \cos\varphi}} \\ \cos\Psi_2 = \dfrac{\kappa_2 U_1 + U_2 \cos\varphi}{\sqrt{\kappa_2^2 U_1^2 + U_2^2 + 2\kappa_2 U_1 U_2 \cos\varphi}} \end{cases}. \quad \text{(S5)}$$

The eigenvalue $\omega\ (k_x)$ of eq. (S3) can then be calculated from:

$$\begin{aligned}\left[\omega(k_x) - \omega_1\right]\left[\omega(k_x) - \omega_2\right] = &\left(V^2 + A_1A_2 + v_1v_2k_x^2\right) \pm \\ &2\sqrt{A_1A_2}V\sqrt{\frac{1+\cos\left(\Psi_1 - \Psi_2\right)}{2} + \frac{v_1v_2k_x^2}{A_1A_2}}\end{aligned}. \quad \text{(S6)}$$

Four eigenvalues at $k_x = 0$ are given by:

$$\begin{aligned} E_1^{(0)} &= \frac{\omega_1 + \omega_2 + \sqrt{\Delta_1}}{2}; E_2^{(0)} = \frac{\omega_1 + \omega_2 - \sqrt{\Delta_1}}{2} \\ E_3^{(0)} &= \frac{\omega_1 + \omega_2 + \sqrt{\Delta_2}}{2}; E_4^{(0)} = \frac{\omega_1 + \omega_2 - \sqrt{\Delta_2}}{2} \end{aligned}, \quad \text{(S7)}$$

where $\begin{cases} \Delta_1 = \left(\omega_1 + \omega_2\right)^2 - 4\left\{\omega_1\omega_2 - \left(V^2 + A_1A_2\right) - \sqrt{2A_1A_2V^2\left[1+\cos\left(\Psi_1 - \Psi_2\right)\right]}\right\} \\ \Delta_2 = \left(\omega_1 + \omega_2\right)^2 - 4\left\{\omega_1\omega_2 - \left(V^2 + A_1A_2\right) + \sqrt{2A_1A_2V^2\left[1+\cos\left(\Psi_1 - \Psi_2\right)\right]}\right\} \end{cases}$. (S8)

The curvature (i.e., second derivative of the dispersion characteristic) based on eq. (S6) is given by:

$$\frac{d^2\omega}{dk_x^2}\left(2\omega-\omega_1-\omega_2\right)+2\left(\frac{d\omega}{dk_x}\right)^2=2v_1v_2\pm2\sqrt{A_1A_2}V\cdot$$
$$\left\{\frac{\frac{v_1v_2}{A_1A_2}}{\sqrt{\frac{1+\cos\left(\Psi_1-\Psi_2\right)}{2}+\frac{v_1v_2k_x^2}{A_1A_2}}}-\frac{\left(\frac{v_1v_2k_x}{A_1A_2}\right)^2}{\left(\frac{1+\cos\left(\Psi_1-\Psi_2\right)}{2}+\frac{v_1v_2k_x^2}{A_1A_2}\right)^{3/2}}\right\}$$

. (S9)

$d\omega/dk_x=0$ and $d^2\omega/dk_x^2=0$ must be satisfied at $k_x=0$ for a flat band. Thus, a flat band (i.e., zero curvature) is obtained when

$$\cos\left(\Psi_1-\Psi_2\right)=\frac{2V^2}{A_1A_2}-1. \tag{S10}$$

The flat band is obtained when high orders of derivatives vanish. The third derivative of the dispersion characteristic at $k_x=0$ is given by:

$$\frac{d^3\omega}{dk_x^3}\left(2\omega-\omega_1-\omega_2\right)+6\frac{d\omega}{dk_x}\frac{d^2\omega}{dk_x^2}=0. \tag{S11}$$

We can then easily verify that the infinite derivative of the dispersion characteristic vanishes at $k_x=0$ ($d^n\omega/dk_x^n=0\left(n\geq1,n\in Z\right)$). Thus, the condition of flat-band generation is $\cos\left(\Psi_1-\Psi_2\right)=2V^2/A_1A_2-1$. If we neglect the diffractive coupling between the evanescent fields of one grating and the waveguide modes of the other grating, we assume that $\kappa_1=\kappa_2=0$. The previous condition becomes:

$$\cos\varphi=\frac{2V^2}{U_1U_2}-1. \tag{S12}$$

S-II. Robustness of the high conversion efficiency of THG under a Gaussian beam incident at different angles

The flat-band-based η_{THG} is robust, reaching approximately two orders of magnitude higher than the dispersive counterpart at a large operating NA, reaching

approximately 0.65 and 0.43 for normal and oblique incidence (with the maximum incident angle reaching 20°), respectively, as shown in the main text. This contrast is robust under a Gaussian beam with NA = 0.43 incident at different angles, as shown in Figure S1(a). The flat-band-based η_{THG} will be 1.5 to 3 orders of magnitude higher with θ_G = 0°, 5°, 10°, 15°, and 20°,, as shown in Figure S1(a). The η_{THG} spectrum of the flat-band metagratings as a function of the fundamental frequency is shown in Figure S1(b) when the Gaussian beam (the divergence angle θ_d = 20°, and the intensity of the axial component $I_G = 0.25\ \mathrm{GW/cm^2}$) is normally incident. The highest η_{THG} reaches approximately 0.16 at the fundamental resonant frequency.

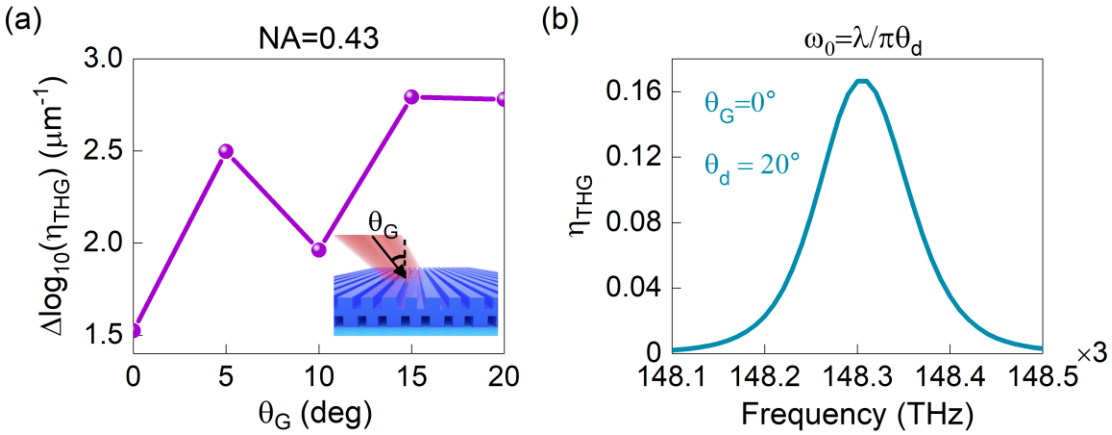

Figure S1 (a) The order of THG enhancement $\Delta log_{10}(\eta_{THG})$, defined as the difference between the logarithmic efficiency between the flat-band metagrating and its dispersive counterpart. (b) The THG conversion efficiency spectrum of the flat-band metagratings as a function of the fundamental frequency when the Gaussian beam is normally incident. $\omega_0 = \lambda/\pi\theta_d$ is the waist radius of the Gaussian beam, and the THG conversion efficiencies are all normalized by the total thickness of the structure.

S-III. Robustness of the flat-band-based higher nonlinear conversion efficiency within the same operating angular range when possible fabrication deviation is introduced

We calculated the total THG conversion efficiencies of the flat- and

dispersive-band-based metagratings with simultaneous incidence of five plane waves (θ = 0°, 5°, 10°, 15°, and 20°) in the main text. The total nonlinear conversion efficiency assisted by the flat band [the band covering a 20-degree operating angle in the black box of Figure S2(a)] is an order of magnitude higher than that of the dispersive band, as shown in Figure S2(d) [the same figure as Figure 4(c) in the main text]. To prove the robustness of the proposed efforts, which includes the flat band obtained and the flat-band-based higher nonlinear conversion efficiency compared with the dispersive-band-based counterpart, we discuss the influences of two possible typical fabrication deviations and provide robustness information. In particular, we increase the parameter F by 0.02 and S by 0.04, corresponding to comb widths in the metagrating (w_1 and w_2) approximately 10 nm wider and a layer misalignment δ of approximately 20 nm more. The TE2 band is still flat in the vicinity of the Γ point, as shown in Figure S2(b). The black box in Figure S2(b) covers a 20-degree operating angle, where the band is almost flat. The total nonlinear conversion efficiency assisted by the flat band [Figure S2(b)] is still an order of magnitude higher than that of the dispersive band, as shown in Figure S2(e), although the highest total resonant frequency will shift. We also decrease the parameter F by 0.02 and S by 0.04, corresponding to comb widths in the metagrating (w_1 and w_2) narrowed by approximately 10 nm and a layer misalignment δ approximately 20 nm less. The TE2 band is still flat in the vicinity of the Γ point, as shown in Figure S2(c), with the black box in Figure S2(c) covering a 20-degree operating angle. The total nonlinear conversion efficiency assisted by this flat band is still an order of magnitude higher than that of the dispersive band, as shown in Figure S2(f), although the highest total nonlinear conversion efficiency assisted by the flat band [Figure S2(c)] is lower than that of Figure S2(d) and (e), with a shift in the total resonant frequency.

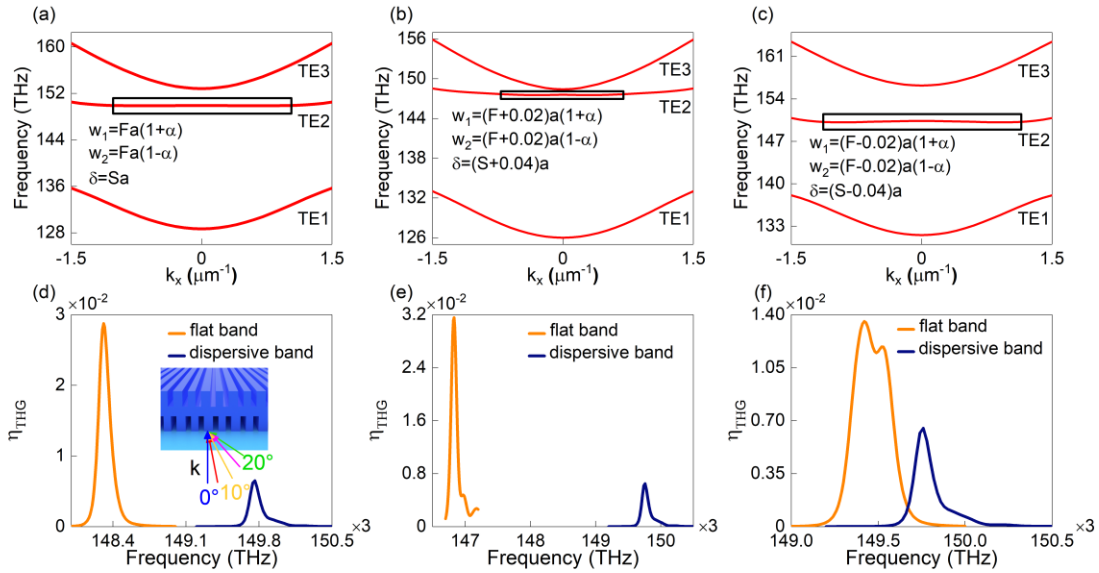

Figure S2 (a)-(c) Calculated three TE bands along the kx axis with the TE2 band flat in the vicinity of the Γ point. (d)-(f) Total ηTHG spectra of the flat- [corresponding to (a)-(c)] and dispersive-band metagratings as a function of the harmonic frequency with simultaneous incidence of five plane waves (θ = 0°, 5°, 10°, 15°, and 20°), as depicted in the inset of (d). The black boxes in (a)-(c) all cover a 20-degree operating angle, where bands are almost flat. The structural parameters of (a) and (d) have been provided in the main text.

S-IV. The comparison of THG phases of the flat band and the dispersive band within wide operating angles

We excite several typical resonances on this flat band and investigate their corresponding nonlinear field distributions within wide operating angles. Figure S3(a)-(c) show comparative field distributions E_y^{TH} (phases) of the flat-band-based THG with incident angles of 6°, 13°, and 20° at resonant frequencies, which guarantees constructive superposition in addition to good spectral overlap. The good spectral overlap of the dispersive-band-based THG conversion efficiency spectra is guaranteed when the pumped incident angles range from -5° to 5°. We excite several typical nonlinear fields within wide operating angles at a resonant frequency of θ = 5° (149.79 THz) on this dispersive band to guarantee spectral overlap. Figure S3(d)-(f)

show field distributions E_y^{TH} (phases) of the dispersive-band-based THG with incident angles of 5°, 12.5°, and 20°, where field enhancement is successively reduced by an order of magnitude from left to right. Although the good spectral overlap at 149.79 THz is guaranteed, and constructive superposition is not guaranteed. Thus, the total nonlinear conversion efficiency assisted by the dispersive band is lower than that of the flat band.

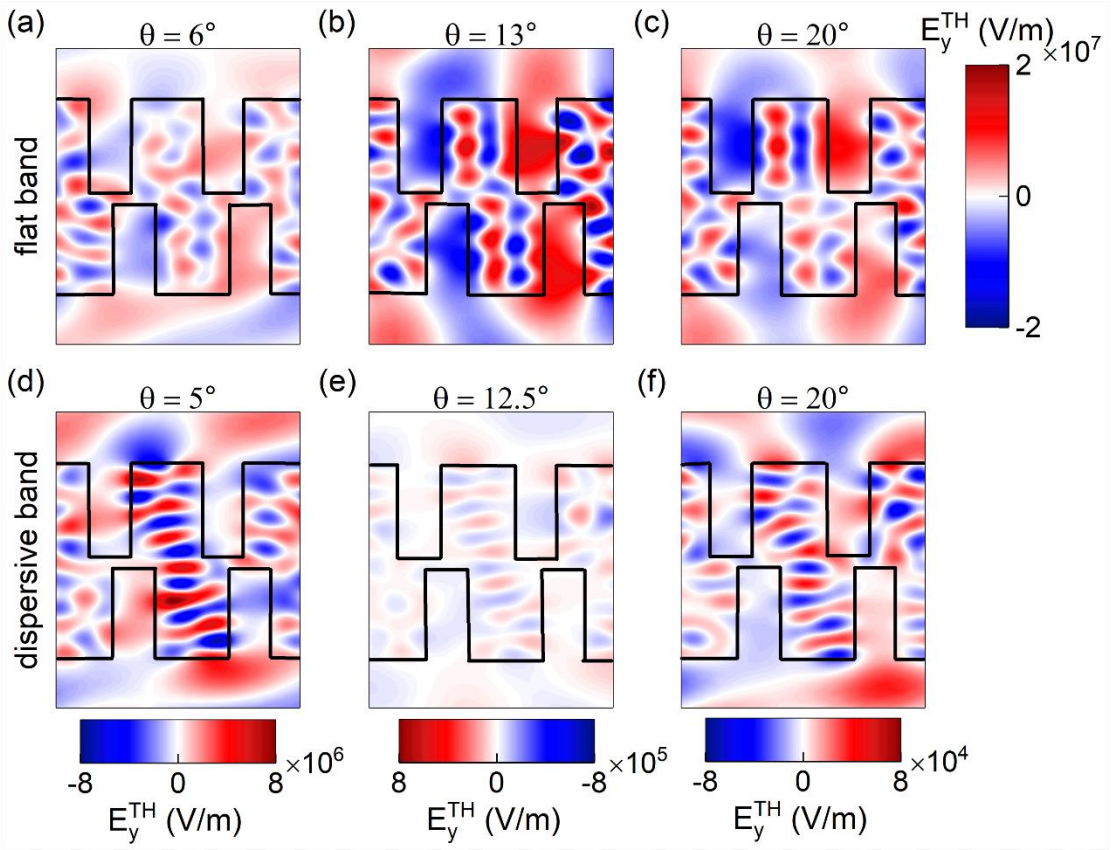

Figure S3 (a)-(c) Harmonic electric field distributions (y component) E_y^{TH} at resonant frequencies in the flat band under incident angles of $\theta = 6°$, 13°, and 20° (left to right). (d)-(f) Harmonic electric field distributions (y component) E_y^{TH} at the resonant frequency of θ = 5° (149.79 THz) on the dispersive band under incident angles of $\theta = 5°$, 12.5°, and 20° (left to right). Both the flat-band and dispersive-band metagratings are excited by a TE plane wave with intensity I_0 = 0.047 GW/cm^2.